Chapter 4

Introducing New Coating Material Alloy with Potential Elements for High Corrosion Resistance for Oil and Gas Application

Mitra Akhtari-Zavareh and
Ahmed Aly Diaa Mohammed Sarhan

Additional information is available at the end of the chapter

http://dx.doi.org/10.5772/64483

Abstract

In petroleum and petrochemical industries, offshore and onshore systems have to function in an aggressive environment that exposes the production equipment components to thermal cycling and wear and corrosion. Although maintenance of material degradation in oil and gas is costly, internal and external parts of the equipment and pipelines must be well inspected and continually maintained. For this reason, highly advanced corrosion and wear–monitoring systems must be installed in the critical areas of the plant to protect pipes and equipment from seawater and crude oil. Therefore, researchers are in search of advanced materials and methods that could be applied in oil and gas pipelines and accessories for increasing their working time. The common manufacturing processing method for improving the surface of piping and accessories is overlay welding or cladding. This method has some limitations, such as its limitation for choosing materials. In addition, the high temperature of welding causes some defects on the final surface, such as thermal residual stress, cracking, and distortion in the substrate. The method is also time consuming and costly. However, the coating method provides a blend of unique properties with low cost. Thermal spray methods are cold spraying techniques that have a considerably less thermal stress, residual stress, and other defects. Among different thermal spray coating techniques, high-velocity oxygen fuel (HVOF) and plasma are the most commonly used thermal spraying coating processes to produce anti-wear and corrosion coatings with different types of materials such as metal, alloys, and ceramic composite . Furthermore, HVOF and plasma thermally sprayed coating processes induce microstructure heterogeneities, which increase the corrosion and wear resistance. In this research, one type of alloy with chemical composition NiCrCoAlY was chosen for increasing corrosion resistivity of carbon steel piping. A corrosion behavior of coated samples in seawater was investigated for 30 days. Potentiodynamic polarization and electrochemical impedance

spectroscopy (EIS) results indicated that these types of alloys protected the surface of carbon steel piping from harsh environments. However, the corrosion protection of NiCoCrAlY deposited by HVOF technique is higher than a plasma coating technique.

Keywords: carbon steel piping surface, thermal spray coating techniques, alloy, corrosion

1. Literature review

Corrosion is generally defined as the destructive disintegration process through which a metal is gradually destroyed by electrochemical reactions with the environment [1]. There is no hard and fast rule to classify corrosion, but it can normally be divided into two main groups, uniform and localized corrosion [2]. In uniform corrosion, damage occurs on the entire surface at a uniform rate. In localized corrosion, damage occurs on localized spots due to heterogeneities in the material microstructure (galvanic, intergranular, and dealloyed) and the environment (crevices and hydrogen damage). Localized stress (stress corrosion cracking, corrosion fatigue, and fretting) and the geometry of closed chemical fluid flow system parts (erosion and cavitation) also cause localized corrosion damage [3, 4].

Corrosion damage depends on the extent of particular factors, e.g. aggressive ions or stress amplitude.

Corrosion has huge economic and environmental impact on infrastructures worldwide such as highways, bridges, oil and gas industries, chemical processing, and water and wastewater systems. Corrosion cannot be fully eliminated but its effects can be minimized using different protection and prevention methods [5]. The direct cost attributed to corrosion damage has been estimated in the order of 3–4% of industrialized countries' gross national product (GNP) [6].

According to the National Association of Corrosion Engineers (NACE), the global corrosion cost, through direct and indirect losses, was $US 552 billion in 2001, which increased to $US 1.3 trillion in 2009 [7]. Direct and indirect damage to the environment is massive if corrosion-related problems are overlooked in sensitive oil/gas industries and nuclear power plants. For instance, radiation and poisonous gas leakage due to severe pitting in nuclear plants can put workers' health at risk [8].

Corrosion measurement and prevention cover a large field of technical activities such as measuring corrosion rate; controlling physical parameters like temperature, pH, and pressure stress; protecting against corrosion like cathodic and anodic protection [9]; chemical dosing; and prevention by material selection or organic/inorganic coatings. Measuring corrosion rate by weight loss is one of the corrosion testing methods commonly used since the past till now [10]. A material is exposed to an environment in which it needs to be in service for a prolonged time (90 days). The corrosion rate is measured from the net weight loss per unit time, i.e. difference in weight before and after the exposure divided by exposure time. In this way, corrosion damage can be assessed for the future by extrapolating the weight loss results. With

http://dx.doi.org/10.5772/64483

advancements in electrochemical sensor technology, different sorts of resistance probes, linear polarization resistance probes, and H_2 evolution probes are used for monitoring corrosion systems [11, 12].

Metallic and nonmetallic coatings along with cladding or surface modifications are also common corrosion prevention methods. Their effective use depends on carefully selecting and regular service monitoring of corrosion. Corrosion prevention, monitoring, and testing can save billions of dollars besides minimize hazards [5, 6].

In oil and gas, many components, such as valve, wellhead, Xmass tree, exchanger, and so on, exposed to the harsh environments and cause the long life of equipment significantly decreased. For this reason, choosing a suitable alloy that has a specific properties depend on environment is essential for increasing corrosion resistivity of equipment [13].

The selection of corrosion resistant alloys is an important step that is directly affected on the long life system. Because, any mistakes for choosing the materials it make some issues for system [5, 13]. Companies with high research facilities first simulate a certain part of the field environment under study. Then, a group of alloys selected some different alloys based on the available information. Then, test all the candidate alloys at the same time and finally choose the best alloys for a certain condition. This method can easily take 1–3 years to accomplish at significant cost [6, 14].

Another selection method is literature review on corrosion data that generally applied to the expected fields. It is quickest and cheapest technique because it neglected some group of alloys that is not suitable for specific condition. Then, the selected alloys are tested under specific condition [13, 15]. However, the chance of error in this method is greater than the previous method, e.g., introducing potential for Corrosion Resistance Alloys (CRA) failure or using a more expensive alloy than required [16].

Other resources for material selection are using available standards, such as the 2003 ISO 15156 publications derived from the previous NACE 0175 publication for "sour service." ANSI/NACE MR0175/ISO 15156 gives general information for service in oil and gas productions and in natural gas sweetening plants in hydrogen sulfide (H_2S)-containing environments, and it also recommended some materials in the appropriate design codes, standards, and regulations. Generally, it can be applied to help avoid costly corrosion damage to the equipment itself [13, 17].

Finally, before accepting the final Alloys for specific condition, it is necessary to simulate the field of environment [14, 16].

Temperature, chloride ion concentration, CO_2 and H_2S, environment pH, and the presence or absence of sulfur (S) are some parameters that directly affect the corrosion properties of alloys [18].

These parameters that cause the risk of stress corrosion cracking (SCC), rate of metal solution from pits, and other things are considerably increased [18].

Generally, three items directly affect the corrosion rate of sample, temperature, pressure, and the chloride content in sodium chloride. In order to make the scale for these parameters is universal, centigrade (°C), pounds per square inch, psi and gram/liter, respectively [19].

Furthermore, the absence of oxygen is critical to the application of these alloys under the conditions shown. If the environment has an oxygen (typically greater than 10 parts per billion), the other alloys should be consider [20, 21].

According to the information presented above, nickel alloys have a long life for oil and gas process fluids. Also it has a high performance and relatively low cost, and at the end of the structure's lifecycle, nickel alloys are completely recyclable. For this reason, this alloy is offered for both the environments [9, 22].

The Nickel Cobalt Chromium Aluminum Yttrium family of gas-atomized powders is designed to produce thermal sprayed coatings with excellent high-temperature oxidation and high-temperature corrosion resistance. The presence of cobalt improves coating ductility and high-temperature corrosion resistance. The presence of chromium and yttrium improves oxidation resistance by increasing the activity of aluminum and improving the spallation resistance of the oxide scale. The function of chromium and aluminum is to provide a reservoir that continually replenishes the oxide scale. Maintaining the chromium and aluminum ratio is critical for avoiding coating embrittlement [23, 24].

Adding tantalum to the chemical composition exhibits superior oxidation resistance at high temperatures. This chemical composition can serve as overlay coating on moving and rotating instruments to improve their performance and service life, even under harsh environmental conditions. Gas atomization ensures excellent chemical homogeneity and high purity, which results in consistent coating results. **Figure 1** represents a SEM photomicrograph of Nickel Cobalt Chromium Aluminum Yttrium powder. The SEM photomicrograph shows gas-atomized morphology that is typical of these materials [25].

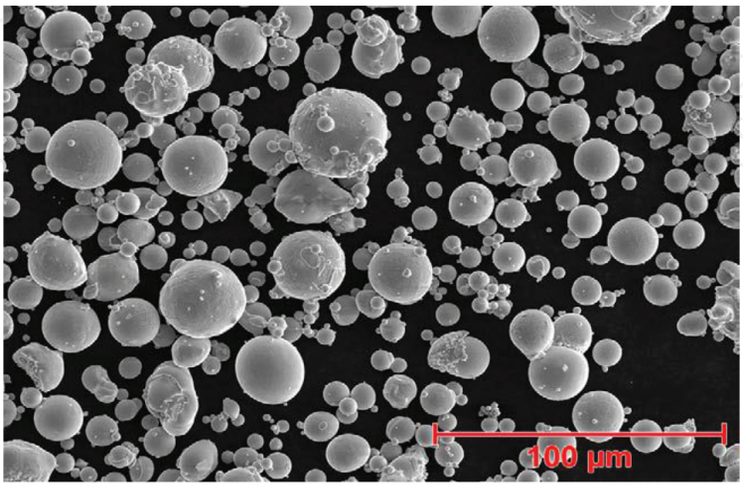

Figure 1. SEM photomicrograph of Nickel Cobalt Chromium Aluminum Yttrium powder morphology.

http://dx.doi.org/10.5772/64483

This chemical composition is a premium grade NiCoCrAlY gas-atomized powder that produces thermal spray coatings with excellent surface resistance against oxidation and corrosion at high temperatures [26].

High-temperature corrosion resistant bond coats act as thermal barrier and oxide-based abradable coatings for hot section components. They also produce superior low oxide coatings that machine well and closely resemble wrought alloys in terms of characteristics [27].

A noteworthy point of preference of thermal spray procedures is to a great degree wide assortment of materials that can be utilized to make coatings. For all intents and purposes, any material that melts without breaking down can be utilized. Another real point of interest is the capacity in most warm splash procedures to apply a covering to a substrate without significantly warming it. In this manner, materials with high melting points can be Joint to the substrate without changing the characteristics or thermal distortions of the parts. A third advantage is the ability, in most cases, to strip and recoat worn or damaged coatings without changing the part's properties or dimensions. Also, applying thin coatings on low-cost substrates results in increased efficiency and cost savings [28–30].

There are five different types of thermal spray coatings: flame spraying, wire arc splashing, detonation gun deposition, plasma spray, and high speed oxy-fuel.

Coating produced by HVOF and plasma processes is characterized by lamellar structure embedded with solid particles, oxide, and inclusions (surface residue from shot blasting or surface cleaning) [14]. Molten or semi-molten particles deform upon hitting the substrate. Deformed particles in the coating are called splats and are approximately 1–20 μm thick. The high striking speed of particles produces compact coating, but some voids/pores still form at the surface and interlamellar particle boundaries [31]. The impaction of solid particles at high speed also adds strength due to the peening effect (relieving tensile stress or adding compression by low level mechanical stresses). The high temperature and presence of oxygen in the environment also cause the formation of oxides. The adhesion between substrate and coating is predominantly by mechanical interlocking [24].

The utilizations of thermal spray coatings are to a great degree changed, yet the vital use classes include upgrading surface wear and/or erosion resistance. Different applications incorporate their utilization for dimensional reclamation, as thermal obstructions, thermal conduits, and electrical channels or resistance; for electromagnetic protection; and improving or retarding radiation. Thermal spray coatings are utilized for all intents and purposes in each industry, including aviation, farming, car, essential metals, mining, paper, oil and gas creation, chemicals and plastics, and biomedicine [25].

2. Methodology

The substrate material used is carbon steel (S45) because it is one of the most popular materials used in oil piping production in both upstream and downstream domains. The substrate material was supplied by Kelvin Steel, Glasgow, with the chemical composition in percentage

as follows: C, 0.42–0.50; Mn, 0.5–0.80; Si, 0.17–0.37; Cr (max%), 0.25; Cu (max%), 0.25; Ni (max %), 0.25; S (max%), 0.035; P (max%), 0.035; and Fe balance.

For the layer deposited onto the carbon steel surface, gas-atomized and spheroidal NiCoCrAlTaY powders with nominal size ranges of 45+11 and 37+15 μm, respectively, were used for plasma and HVOF methods.

For increasing the adhesion of deposited layer to substrate, the surface preparation is a very important step. Roughness of sample directly affects the adhesion of deposited layer, which can be controlled by different parameters such as blasting pressure, angel, and so on. [32].

Grit blasting was carried out with a high efficiency sand blaster with Alumina grit (size 10–20 mesh), 8/10 mm nozzle, and operating at a blasting pressure of >0.5 MPa. The distance between substrate and nozzle was 150 mm with a 30° angle. The grit blasting time was dependent on obtaining the required surface roughness. Upon grit blasting completion, powders with different chemical compositions were sprayed using HVOF and/or plasma gun systems.

The coating thickness selected for all samples in this research after trial and error was approximately 400 μm. Generally, increasing some initial parameters, such as arc current, power feed rate, and so on, helps increase the thermal spray coating thickness.

For the deposition of this powder by HVOF machine, a Model 9MP machine was employed. **Table 1** shows the parameters for HVOF coating. For plasma coating, the same specific setup was used as for HVOF coating in this material powder group. The setup of powder coated by plasma machine is tabulated in **Table 2**.

Model: 9MP	**DJ2700 hybrid**		
Nozzle	Standard		
Powder port			
Type		DJ2702	
Injector		#9	
Angle		90°	
Suction and spreader		L/L	
Gases	Pressure (psi)	Flow (FMR)	SCFH
Oxygen	155	282.2	645
Natural gas (CH_4)	110	140.2	320
Carrier gas (N_2)[1]	105	350	799
Spray distance	254 mm (10″)		
Spray rate	38 g/min (5 lb./h)		

[1]Using nitrogen as a shroud gas will reduce coating oxide content.

Table 1. Parameters of NiCrCoAlY powder for HVOF coating.

http://dx.doi.org/10.5772/64483

Gun	F4		
Nozzle	Standard		
Powder port			
Type	#2 (1.8 mm/0.071″)		
Gauge	#6		
Angle	90°		
Disc rpm[1]	23		
Suction and spreader	L/L		
Gases	Pressure (psi)	NLPM	SCFH
Primary (air)	75	65	1218
Secondary (H_2)	50	14	32
Carrier (air)	100	2.3	5.2
Amps	600		
Voltage	66		
Spray distance	114–140 mm (4.5–5.5″)		
Spray rate	40–57 g/min (5.3–7.5 lb./h)		

[1]As a starting point, adjust to indicate spray rate.

Table 2. Parameters of NiCrCoAlY powder for plasma coating.

The coating morphology was observed through a high resolution FEI Quanta 200F field emission scanning electron microscope (FESEM). Using an EDX-System (Hitachi SU8000) instrument attached to a FESEM instrument, energy dispersive X-ray (EDAX) analysis was performed to investigate the elemental composition of the samples.

The surface of the substrate and coated samples before and after corrosion was also studied by a relatively destructive method. The X-ray diffraction (XRD) equipment is an Empyrean X-ray diffractometer with Cu Ka radiation (k = 1.54178 A operating at 45 kV, 30 mA, 0.026° step size, and scanning rate of 0.1 s 1 in a 2 h range from 10° to 90°).

For measuring the corrosion rate of coated sample, electrochemical techniques, such as DC (polarization) and AC (impedance), were used and applied using a potentiostat/galvanostat model AutoLab PGSTAT30 from Ecochemie (Netherlands) [33]. Polarization experiments were performed using a three-electrode cell, where the samples were the working electrode (WE) while a platinum wire and saturated calomel electrode (SCE) was the counter and reference electrodes, respectively. The electrolyte was 3.5% NaCl. In this test, the linear scan voltammetry, corrosion current (I_{corr}), and corrosion potential (E_{corr}) were calculated from the Tafel plots with a scan rate of 0.001 Vs^{-1}.

A frequency range of 10^5–10^{-2} Hz with amplitude potential of 5 mV vs SCE was used to conduct electrochemical impedance spectroscopy (EIS). To obtain the charge transfer resistance values

across the electrode-electrolyte interface that could relate to parameters from the polarization output, simulations with analog circuits were performed with the experimental data. Having been installed in a computer interfaced with a potentiostat, general purpose electrochemical software (GPES) and frequency response analyzer (FRA) were used to run the AC and DC techniques, respectively.

3. Results, analysis and discussion

3.1. Microstructural analysis of surface

Figure 2 displays FESEM micrographs of plasma and HVOF-coated samples before corrosion testing. The top view image indicates a relatively dense, uniform, and crack-free coating deposited on the substrate. However, the HVOF-coated samples have a semi-uniform surface compared to the plasma-coated samples.

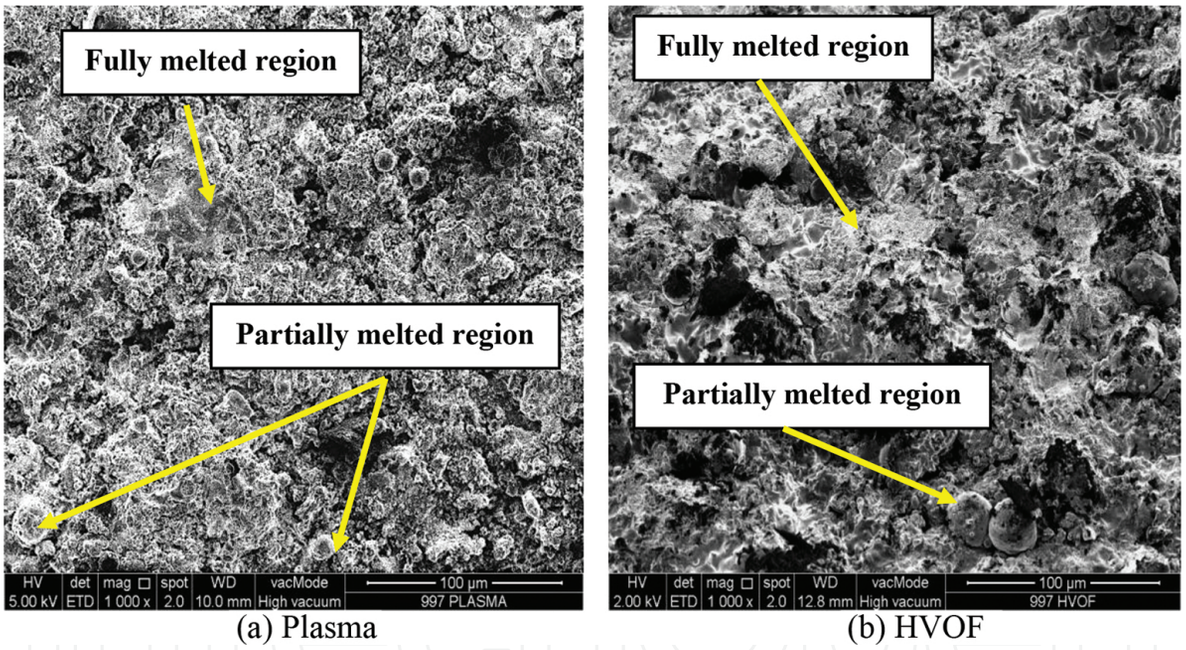

Figure 2. FESEM of NiCoCrAlY-coated samples at different magnifications: (a) plasma and (b) HVOF.

A small amount of semi-molten and nonmolten particles is visible in the fully melted region (Ni) area. The presence of semi-molten and nonmolten particles provides the coating with high bonding strength and good wear resistance [34, 35]. A few pores appear in black in the micrographs of both types of coating. The porosity size and Average number of porosity with the HVOF method are greater than with plasma.

The coatings deposited by plasma spray (**Figure 2a**) exhibit the most visible defects. Shrinkage of the molten droplets, as they splat onto the substrate and rapidly solidify, is one of the main causes of porosity and visible defects in plasma spray coatings. Coatings deposited by HVOF

http://dx.doi.org/10.5772/64483

(**Figure 2b**) feature the most desirable structure with minimal porosity, absence of cracks, and a clean interface with the substrate. The finer pores within HVOF coating demonstrate the superior compaction and deposition of particles during spraying. Also, HVOF coating has a rough surface due to the overlap of different splats and the roughness of each single splat [36, 37].

X-ray diffraction patterns and EDX for NiCoCrAlY plasma and HVOF-coated samples are shown in **Figure 3**. According to the coated samples in **Figure 3a** and **b**, Only three phases were detected γ (Co, Ni, Cr), β(Co, Ni, Y)Al, and Al_2O_3. The morphology of the coatings consists of single-phase splats separated by Al_2O_3veins as a result of the oxidation occurring in the deposition process.

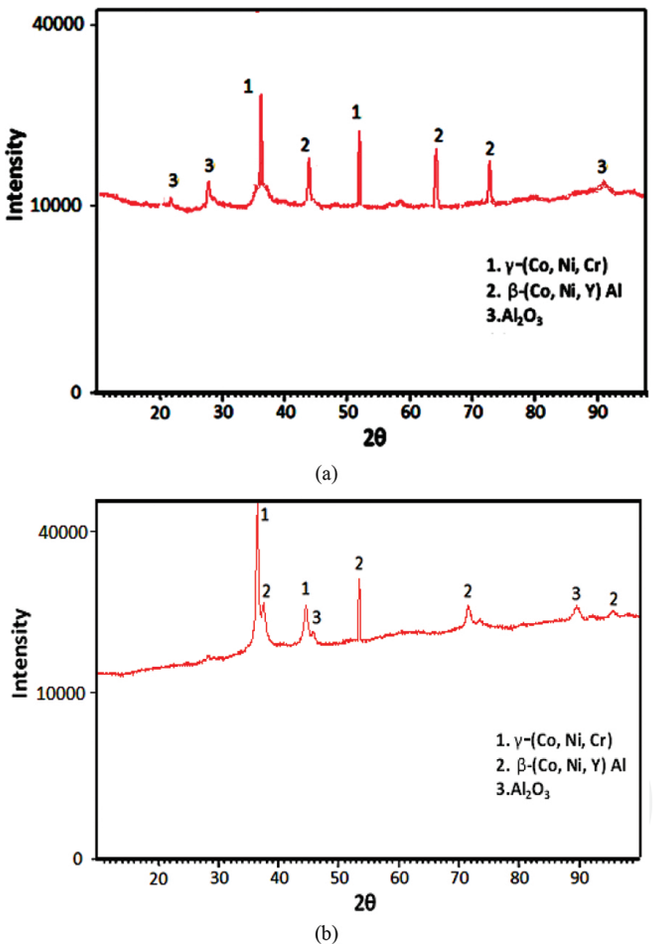

Figure 3. X-ray diffraction patterns for NiCoCrAlY-coated samples with: (a) plasma and (b) HVOF.

Previous studied showed the samples that coated with NiCoCrAlY by vacuum plasma coating(VPS) have high performance. Because it can provide good adhesion to the metallic substrate with high density, while this method is more expensive rather than other techniques of thermal spray coatings. For this reason, high-velocity oxygen fuel (HVOF) has a good option for disposition of NiCoCrAlY alloys instead of VPS. However, existing the free oxygen in the

combustion gas causes increasing homogeneity in the melted powders and remove Oxidation particles, because they need high temperature. The aluminum and yttrium elements in the metallic powder have high affinity with oxygen and are thus easily oxidized during thermal spraying; consequently, the coatings have high oxide content [38–42].

3.2. Electrochemical corrosion analysis

The open circuit potential (OCP) of coated samples for day 3 and day 30 is shown in **Figure 4**. The plasma-coated sample (blue) shows the potential moved from −0.421 on day 3 toward noble regions to −0.341 at the end of that period, and the OCP of the HVOF-coated sample (red) was more negative compared to the plasma-coated sample, with a change from −0.305 on day 3 to −0.413 on day 30.

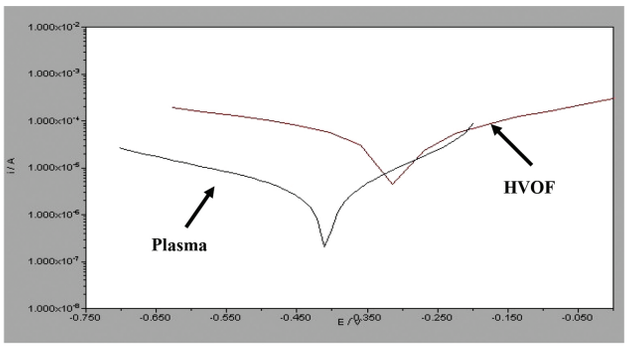

(a) 3rd day experiments

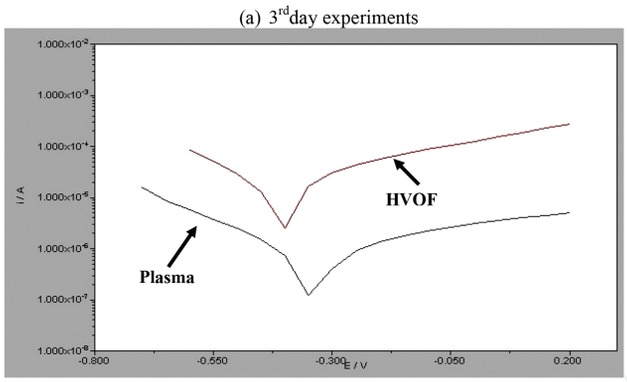

(b) 30th day experiments

Figure 4. Polarization curves (log I vs E) of NiCoCrAlY with plasma and HVOF methods for (a) 3rd day and (b) 30th day experiment.

The charge transfer resistance R_{ct} was consistent with the OCP values from polarization measurements and I_{corr} illustrated in **Table 3**. It can be seen that the R_{ct} for plasma-coated samples changed from 11.735 to 10.098 kΩ from day 3 to day 30, and for the HVOF-coated samples, it changed from 12.193 to 8.242 kΩ. The higher R_{ct} (EIS data) is due to the greater resistance to charge transfer across the electrode-electrolyte interface, which is consistent with the positive OCP result values belonging to the plasma-coated sample. From the computer simulations for the plasma-coated sample, the R_s (QR) circuit diagram accurately matches the experimental data. Only one semicircle is observed in the Nyquist plot (**Figure 5a** and **c**).

http://dx.doi.org/10.5772/64483

Day	Plasma-coated sample				HVOF-coated sample			
	OCP		I_{Corr}/A (×10^{-5})	R_{CT}/kOhm	OCP		I_{Corr}/A (×10^{-5})	R_{CT}/kOhm
	Mean	SD			Mean	SD		
3	−0.421	0.00061	5.683	11.735	−0.305	0.00054	5.267	12.193
6	−0.413	0.00052	5.701	11.380	−0.319	0.00050	5.326	11.871
9	−0.404	0.00072	5.784	11.034	−0.328	0.00071	5.635	10.714
12	−0.389	0.00088	5.832	10.784	−0.289	0.00074	4.897	11.341
15	−0.379	0.00069	5.975	10.514	−0.340	0.00069	5.593	10.891
18	−0.367	0.0010	6.030	10.321	−0.367	0.00081	5.772	10.462
21	−0.360	0.00092	5.436	10.989	−0.378	0.00073	5.829	9.843
24	−0.354	0.00085	5.591	10.679	−0.382	0.0005	6.084	9.245
27	−0.348	0.00074	6.096	10.364	−0.395	0.0011	6.203	8.884
30	−0.341	0.00092	6.231	10.098	−0.413	0.00089	6.289	8.242

Table 3. OCP, I_{corr}, and R_{CT}/kOhm of NiCoCrAlY samples with plasma and HVOF coating methods in 3.5% NaCl solution for 30 days.

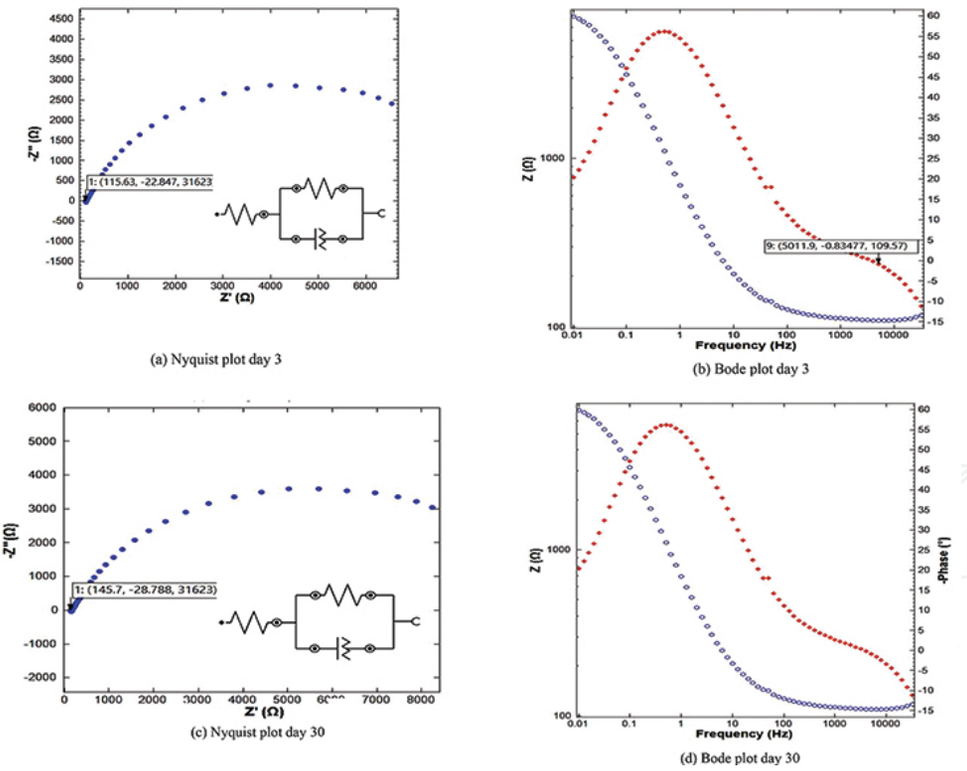

Figure 5. EIS of NiCoCrAlY plasma-coated samples. (a) Nyquist plot day 3, (b) Bode plot day 3, (c) Nyquist plot day 30, and (d) Bode plot day 30.

The Bode phase diagrams of the plasma-coated samples (**Figure 5b** and **d**) show one-phase maxima, consistent with the presence of one semicircle in the Nyquist plots from **Figure 5a**

and **c** with R_s (Q_1R_1) circuit. The R_s (QR) circuit diagram accurately matches the start day of the plasma-coated samples. Only one semicircle and one maximum phase were observed in the Nyquist and Bode plots (**Figure 5a** and **b**). **Figure 6a** and **b** shows that the R_s (QR) circuit diagram accurately matches the experimental data at the beginning of measurement. Whereas for the HVOF-coated samples, at the end of the period, the equivalent circuit R_s (Q_1 [R_1(Q_2R_2)] accurately fits the experimental data for HVOF coating, because two semicircles and maxima phases were observed in the Nyquist and Bode plots (**Figure 6c** and **d**). The resistance between RE and WE is the solution resistance R_s, which is in series with two time constants (parallel arrangement of R and Q) that are also in series.

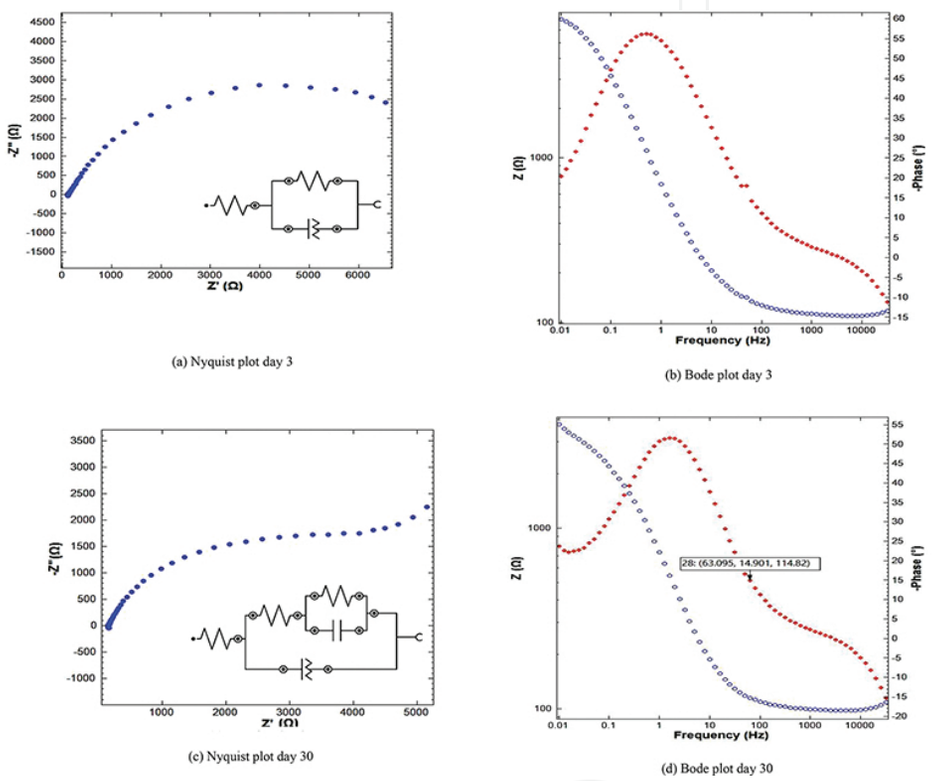

Figure 6. EIS of NiCoCrAlY HVOF-coated samples. (a) Nyquist plot day 3, (b) Bode plot day 3, (c) Nyquist plot day 30, and (d) Bode plot day 30.

It can be seen that the Nyquist plot (**Figure 5c**) is a "depressed semi-circle" with the center of the circle below the x-axis [43–45]. Q_1 is parallel to R_1. $R_1$is the polarization resistance of the area at the substrate/coating interface where corrosion occurs. Also, Q_2 is in parallel with a charge transfer resistor R_2, corresponding to the pores on the coated layer surface. The main reason for the higher R_{ct} of the plasma-coated sample than the HVOF-coated sample at the end of the period is the presence of a bigger oxide layer on top of the plasma-coated samples that protects the deposited layers from electrolyte penetration to the interface.

In these simulations, the plasma coating had higher charge transfer resistances, R_{ct}, than the HVOF coating due to the higher resistance against corrosion. The charge transfer resistance, R_{ct}, values for plasma and HVOF-coated samples are presented in **Table 3**.

http://dx.doi.org/10.5772/64483

According to **Table 3**, the corrosion current density of plasma-coated samples increased from 5.683×10^{-5} to 6.030×10^{-5} from day 3 to day 18, and then suddenly dropped to 5.436×10^{-5}A on day 21. After that, it rose again up to 6.231×10^{-5}A on day 30. The corrosion current density for HVOF-coated samples moved from 5.267×10^{-5} to 5.635×10^{-5} on day 3 to day 9, but suddenly dropped to 4.897×10^{-5}A on day 12. From the middle of the period until the end, the current density increased from 5.593×10^{-5} to 6.289×10^{-5}A. The decreasing amount of corrosion current density related to the oxide layer created on top of the deposited layer protected the samples from the corrosive environment. Therefore, the amount of R_{ct} over this period increased.

3.3. Microstructural analysis of corrosion

FESEM micrographs of both coated sample types after 30 days of immersion in crude oil and seawater are shown in **Figures 7** and **8**. According to **Figures 7a** and **8a**, when samples were exposed to the oil environment, the corrosion rate on the coated samples' surface was lower than in NaCl electrolyte (seawater) solution. According to **Figure 7**, the amount of pitting corrosion on the plasma samples was less than the HVOF samples, because there were fewer fine holes produced than on the HVOF samples.

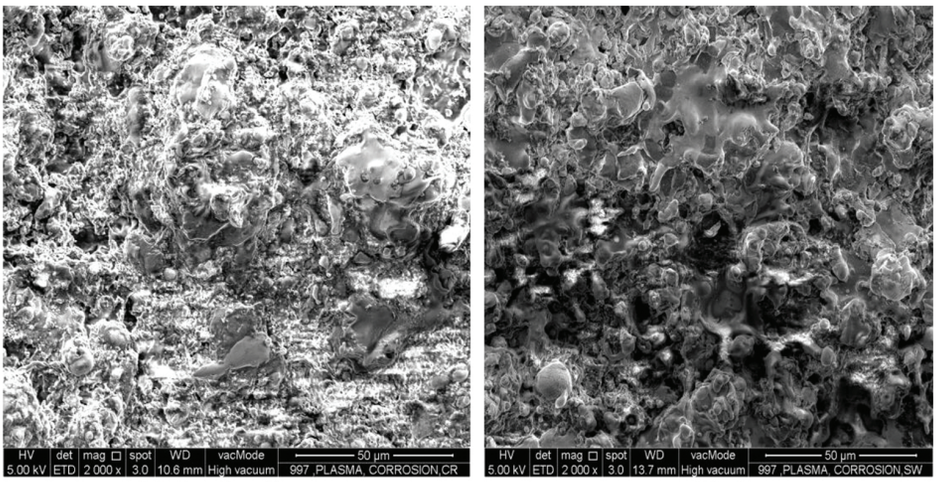

(a) Crude oil (b) Seawater

Figure 7. FESEM micrographs of NiCoCrAlY plasma-coated sample surfaces after 30 days: (a) in crude oil and (b) in seawater.

In **Figure 8**, the HVOF-coated samples corroded significantly after 30 days and large holes appeared on their surface. This coating displayed evident crevices and pitting corrosion in the microstructure containing intersplat porosity, that was detected on the top surface of HVOF-coated samples by previous studies [46, 47]. Also, the size and amount of corroded area inside NaCl solution (seawater) is obviously greater than in the crude oil.

Regarding **Figures 7** and **8**, there is a big difference between the corroded and uncorroded samples with the HVOF coating method in both environments, whereas in plasma-coated samples, the difference between corroded and uncorroded samples is considerably less than the HVOF method. However, both methods protected the substrate from corrosion.

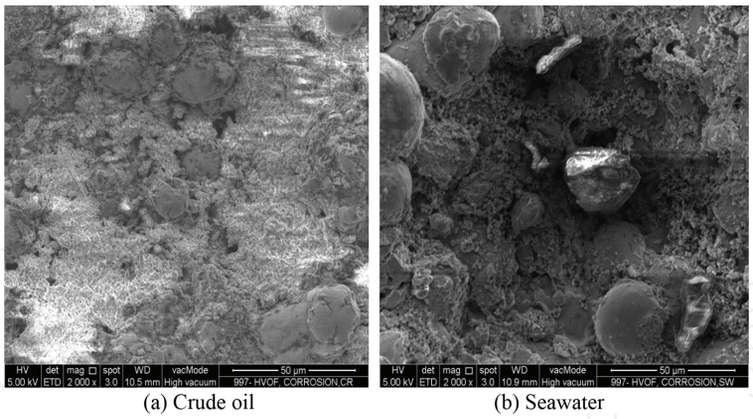

(a) Crude oil (b) Seawater

Figure 8. FESEM micrographs of NiCoCrAlY HVOF-coated sample surfaces after 30 days: (a) in crude oil and (b) in seawater.

Generally, there are several factors affecting corrosion resistance, including adhesion force between coating layer and substrate, cooling rate, generation of oxides and compounds, and porosity [48, 49]. The NiCoCrAlY alloy has an excellent corrosion resistance and oxides generated affect chemical stability, bond strength, and durability. As it has high adhesion to the base metal and creates a dense oxide layer, it yields high durability [50].

4. Conclusion

Morphological, microstructural, and compositional analyses were performed for both coating methods in order to characterize the samples before and after the corrosion tests. The characterization for seawater (3.5% NaCl) and crude oil after 30 days showed that both methods can protect the substrate from corrosion, but the corrosion rate with HVOF is higher than with the plasma coating method. This result suggests that the potential impact of the plasma thermal spraying process against a corrosive environment is better than that of HVOF spraying systems. Therefore, from this chemical composition group, the plasma samples were chosen for corrosion resistivity.

Author details

Mitra Akhtari-Zavareh* and Ahmed Aly Diaa Mohammed Sarhan

*Address all correspondence to: akhtari.mitra@yahoo.com

Department of Mechanical Engineering, Faculty of Engineering Building, University of Malaya, Kuala Lumpur, Malaysia

http://dx.doi.org/10.5772/64483

References

[1] Fantana, F, Goldoni, D & Grandi, G. (1992). Visualization of ribosomal gene activity in oogenesis of Reticulitermes lucifugus (Isoptera: Rhinotermitidae) revealed by silver staining. Cytologia, 57(2), 223-226.

[2] Jones, DA. (1996). Principles and Prevention of Corrosion (2nd ed.): Prentice Hall,The University of Michigan, USA

[3] Perez, N. (2004). Electrochemistry and Corrosion Science: Kluwer Academic. pp. 3. Department of Mechanical Engineering, University of Puerto Rico, USA

[4] Akhtari Zavareh, M, Sarhan, A, Razak, B, & Basirun, WJ. (2015). The tribological and electrochemical behavior of HVOF-sprayed Cr 3 C 2–NiCr ceramic coating on carbon steel, Ceramics International 41, 5387-5396.

[5] Cramer, SD.&Covino, BS. (2003). Corrosion: Fundamentals, Testing, and Protection (Vol. 13A): Materials Park, OH, USA

[6] Cramer, SD&Covino, BS. (2006). Corrosion: Environments and Industries (Vol. 13): ASM International, Materials Park, OH, USA

[7] Setayesh, H, Moradi, H, & Alasty, A. (2015). A comparison between the minimum-order & full-order observers in robust control of the air handling units in the presence of uncertainty. Energy and Buildings, 91, 115-130.

[8] Villalobos, ME, Mizuno, A, Dahl, BC, Kemmotsu, N, & Müller, R-A. (2005). Reduced functional connectivity between V1 and inferior frontal cortex associated with visuomotor performance in autism. Neuroimage, 25(3), 916-925.

[9] Parker, ME,&Peattie, EG. (1984). Pipe Line Corrosion and Cathodic Protection: A Practical Manual for Corrosion Engineers, Technicians, and Field Personnel: Gulf Professional Publishing, Burlington, USA

[10] Younis, AA, Ensinger, W, El-Sabbah, MMB, & Holze, R. (2013). Corrosion protection of pure aluminium and aluminium alloy (AA7075) in salt solution with silane-based sol–gel coatings. Materials and Corrosion, 64(4), 276-283.

[11] Akhtari Zavareh, M, Sarhan AADM, Zavareh, PA, & Basirun, WJ. (2015). Electrochemical corrosion behavior of carbon steel pipes coated with a protective ceramic layer using plasma and HVOF thermal spray techniques for oil and gas, Ceramics International, 42, 3397-3406.

[12] Sampath, S, Jiang, XY, Matejicek, J, Prchlik, L, Kulkarni, A, & Vaidya, A. (2004). Role of thermal spray processing method on the microstructure, residual stress and properties of coatings: an integrated study for Ni–5 wt.% Al bond coats. Materials Science and Engineering: A, 364(1), 216-231.

[13] Craig, BD,&Smith, L. (2011). Corrosion resistant alloys (CRAs) in the oil and gas industry. Nickel Institute Technical Series No. 10073.

[14] Eadie, RL, Szklarz, KE, & Sutherby, RL. (2005). Corrosion fatigue and near-neutral pH stress corrosion cracking of pipeline steel and the effect of hydrogen sulfide. Corrosion, 61(2), 167-173.

[15] Akhtari Zavareh, M, Sarhan, AAD, Bushroa, AR, & Basirun, WJ. (2014). Plasma thermal spray of ceramic oxide coating layer to enhance wear and corrosion resistance of carbon steel for oil and gas application, Ceramics International. 40, 14267-14277.

[16] Javaherdashti, R. (2000). How corrosion affects industry and life. Anti-corrosion Methods and Materials, 47(1), 30-34.

[17] Nešić, D, Tan, Y, Moase, WH, & Manzie, C. (2010). A Unifying Approach to Extremum Seeking: Adaptive Schemes Based on Estimation of Derivatives. 49th IEEE Conference on Decision and Control (CDC),15-17 December, Hilton Atlanta Hotel, Atlanta, GA, USA

[18] Lucci, A, Demofonti, G, & Spinelli, CM. (2011). CO_2 Anthropogenic Pipeline Transportation. Paper presented at the Proceedings of the Twenty-first International Offshore and Polar Engineering Conference, Maui, Hawaii, USA.

[19] Kirk-Othmer (2007), Encyclopedia of Chemical Technology, Volume 25, 5th Edition, Wiley USA.

[20] Lucio-Garcia, MA, Gonzalez-Rodriguez, JG, Casales, M, Martinez, L, Chacon-Nava, JG, Neri-Flores, MA, & Martinez-Villafañe, A. (2009). Effect of heat treatment on H2S corrosion of a micro-alloyed C–Mn steel. Corrosion Science, 51(10), 2380-2386.

[21] Selman, C. (2011). Condensation Corrosion Modelling, Reality and Design in Deep Water Wet Gas Pipelines. Paper presented at the The Twenty-first International Offshore and Polar Engineering Conference.

[22] M. Akhtari Zavareh, A. Sarhan, B. Razak and WJ. Basirun, (2014). Electrochemical Characterizations of Different Ceramic Composite Coatings on Carbon Steel Piping Using High Velocity Oxy-Fuel Spray, Proceedings of the World Congress on Engineering and Computer Science 2014, San Francisco, USA, 22-24 October 2014, Vol. 2, 664-668.

[23] Islak, S, Buytoz, S, Ersöz, E, Orhan, N, Stokes, J, Saleem Hashmı, M, Tosun, N. (2013). Effect on microstructure of TiO_2 rate in Al_2O_3-TiO_2 composite coating produced using plasma spray method, Optoelectronics And Advanced Materials – Rapid Communications, Vol6, No 9-10, p 844-849.

[24] Marple, Basil Richard, Lima, Rogerio S, Moreau, Christian, Kruger, Silvio E, Xie, L, & Dorfman, MR. (2007). Yttria-stabilized zirconia thermal barriers sprayed using N2-H2

and Ar-H2 plasmas: influence of processing and heat treatment on coating properties. Journal of Thermal Spray Technology, 16(5-6), 791-797.

[25] Tuominen, J, Vuoristo, P, Mäntylä, T, Kylmälahti, M, Vihinen, J, & Andersson, PH. (2000). Improving corrosion properties of high-velocity oxy-fuel sprayed inconel 625 by using a high-power continuous wave neodymium-doped yttrium aluminum garnet laser. Journal of Thermal Spray Technology, 9(4), 513-519.

[26] Mumtaz, KA, Erasenthiran, P, & Hopkinson, N. (2008). High density selective laser melting of Waspaloy®. Journal of Materials Processing Technology, 195(1), 77-87.

[27] Torabian, S, Haddad, E, Rajaram, S, Banta, J, & Sabate, J. (2009). Acute effect of nut consumption on plasma total polyphenols, antioxidant capacity and lipid peroxidation. Journal of Human Nutrition and Dietetics, 22(1), 64-71.

[28] Berndt, ML, & Berndt, CC. (2003). Thermal spray coatings. Corrosion: Fundamentals, Testing, and Protection, 13, 803-813.

[29] Berndt, CC. (2001). Thermal Spray 2001: New Surfaces for a New Millennium: Proceedings of the International Thermal Spray Conference: ASM International, Materials Park, Ohio, USA

[30] Akhtari Zavareh, M, Sarhan, AADM, Akhtari Zavareh, P, Razak, BBA, Basirun, WJ, Ismail, MBC. (2016). Development and protection evaluation of two new, advanced ceramic composite thermal spray coatings, Al 2 O 3–40TiO 2 and Cr 3 C 2–20NiCr on carbon steel petroleum oil piping, Ceramics International, 42, 5203-5210.

[31] Al-Fadhli, HY, Stokes, J, Hashmi, MSJ, & Yilbas, BS. (2006). The erosion–corrosion behaviour of high velocity oxy-fuel (HVOF) thermally sprayed inconel-625 coatings on different metallic surfaces. Surface and Coatings Technology, 200(20), 5782-5788.

[32] Mann, BS, & Arya, Vivek. (2001). Abrasive and erosive wear characteristics of plasma nitriding and HVOF coatings: their application in hydro turbines. Wear, 249(5), 354-360.

[33] Hartfield-Wünsch, SE, & Tung, SC. (1994). The Effect of Microstructure on the Wear Behavior of Thermal Spray Coatings: ASM International, Materials Park, OH (United States).

[34] Somasundaram, B, Kadoli, R, & Ramesh, MR. (2014). Evaluation of cyclic oxidation and hot corrosion behavior of HVOF-sprayed WC-Co/NiCrAlY coating. Journal of Thermal Spray Technology, 23(6), 1000-1008.

[35] Wu, YS, Zeng, DC, Liu, ZW, Qiu, WQ, Zhong, XC, Yu, HY, & Li, SZ. (2011). Microstructure and sliding wear behavior of nanostructured Ni60–TiB_2 composite coating sprayed by HVOF technique. Surface and Coatings Technology, 206(6), 1102-1108.

[36] Richer, P, Yandouzi, M, Beauvais, L, & Jodoin, B. (2010). Oxidation behaviour of CoNiCrAlY bond coats produced by plasma, HVOF and cold gas dynamic spraying. Surface and Coatings Technology, 204(24), 3962-3974.

[37] Zhang, Q, Li, C-J, Li, C-X, Yang, G-J, & Lui, S-C. (2008). Study of oxidation behavior of nanostructured NiCrAlY bond coatings deposited by cold spraying. Surface and Coatings Technology, 202(14), 3378-3384.

[38] Yuan, FH, Chen, ZX, Huang, ZW, Wang, ZG, & Zhu, SJ. (2008). Oxidation behavior of thermal barrier coatings with HVOF and detonation-sprayed NiCrAlY bondcoats. Corrosion Science, 50(6), 1608-1617.

[39] Jiang, J, Zhao, H, Zhou, X, Tao, S, & Ding, C. (2012). The effect of ion implantation on the oxidation resistance of vacuum plasma sprayed CoNiCrAlY coatings. Applied Surface Science, 261, 422-430.

[40] Nijdam, TJ, Jeurgens, LPH, & Sloof, WG. (2005). Promoting exclusive α-Al_2O_3 growth upon high-temperature oxidation of NiCrAl alloys: experiment versus model predictions. Acta Materialia, 53(6), 1643-1653.

[41] Zavareh, MA, Hamdi, M, Ghahnavyeh, RR, Roudan, MA, Shafieirad, M. (2013). Fabrication of TiB2-TiC composites optimized by different amount of carbon in the initial Ti-BC powder mixture, Applied Mechanics and Materials, 315, 720-723.

[42] Miguel, JM, Guilemany, JM, & Vizcaino, S. (2003). Tribological study of NiCrBSi coating obtained by different processes. Tribology International, 36(3), 181-187.

[43] Zavareh, MA, Sarhan, AAD, Roudan, MA, Zavareh, PA. (2014) TiC–TiB_2 composites: A review of processing, properties and applications, International Journal of Innovative Research in Science & Engineering, 4, 2347-3207.

[44] Mochizuki, H, Yokota, M, & Hattori, S. (2007). Effects of materials and solution temperatures on cavitation erosion of pure titanium and titanium alloy in seawater. Wear, 262(5), 522-528.

[45] Woo, Y-B, Lee, S-J, Jeong, J-Y, & Kim, S-J. (2014). Evaluation on cavitation characteristics of CoNiCrAlY/ZrO 2–Y2O3 coating layer by atmospheric pressure plasma coating process. Materials Research Bulletin, 58, 78-82.

[46] Zavareh, MA, Sarhan, AAD, Roudan, MA, Zavareh, PA. (2014). A new approach to fabricate TiB_2-TiC composite utilizing self-propagation high temperature via pressure less sintering, International Journal of Engineering & Technology Sciences, 2, 193-203.

[47] Mansfeld, F. (1990). Electrochemical impedance spectroscopy (EIS) as a new tool for investigating methods of corrosion protection. Electrochimica Acta, 35(10), 1533-1544.

[48] Dent, AH, Horlock, AJ, McCartney, DG, & Harris, SJ. (2000). Microstructure formation in high velocity oxy-fuel thermally sprayed Ni–Cr–Mo–B alloys. Materials Science and Engineering: A, 283(1), 242-250.

[49] Zavareh, MA, Sarhan, AADM, Zavareh, PA. (2015). Comparison and wear behavior evaluation of Cr_3C_2-25%NiCr composite coated on carbon steel by two different thermal spray techniques, International Journal of Material Science Innovations, 3, 87-96.

[50] Wei-jie, L, Yong, L, Yan, W, Chao, H,&Hui-ping, T.(2011), Hot corrosion behavior of Ni–16Cr–xAl based alloys in mixture of Na2SO4–NaCl at 600 °C, Transactions of Nonferrous Metals Society of China,Vol.21, No12,p. 2617-2625

IntechOpen

IntechOpen